MANAS Journal of Engineering
ISSN 1694-7398 | e-ISSN 1694-7398

Volume 12, Issue 2, (2024) Pages 224-235
https://doi.org/10.51354/mjen.1586502

A Study on Controllable Mod Exploiting the Intrinsic Symmetry Breaking of Low-symmetry Photonic Crystals

Özgür Önder Karakılınç[1,*]

[1] Pamukkale University, Electrical and Electronics Engineering Department Denizli, Türkiye, okarakilinc@pau.edu.tr, ORCID: 0000-0003-4586-9845

ABSTRACT

Photonic crystals are periodic dielectric structures that create photonic band gaps depending on the geometry of the lattice elements and the material properties. These structures allow light to be easily controlled, guided, and confined due to the tunability and adjustability of their design parameters. Conventional photonic crystals are typically designed with high-symmetry unit cells, while low-symmetry structures are created by breaking this symmetry. Low-symmetry structures are more sensitive to light manipulation and offer greater control and flexibility over light through geometric diversity. This study investigates the resonance effect in a cavity structure composed of a square lattice photonic crystal made of low-symmetry C2-type dielectric rods. The dependence of the resonance mode on the low-symmetry parameters was investigated and it was shown that, in contrast to other studies, mode splitting or merging can be achieved and tuned by exploiting and perturbing the intrinsic symmetry properties of the low-symmetry photonic crystal structure. The band structure, transmission spectra, and resonance frequencies of the low rotational symmetry photonic crystal were obtained using Lumerical and MEEP software. The analysis of resonance splitting and optical properties by symmetry manipulation will contribute to the understanding of light collimation and trapping.

ARTICLE INFO

Research article

Received: 16.11.2024
Accepted: 12.12.2024

Keywords:
Photonic crystals, Low symmetry, Resonance mode

**Corresponding author*

1. Introduction

Photonic crystals (PCs) are artificial materials that exhibit photonic band gaps depending on the geometry of the structure and the refractive index properties, and contain a one-dimensional (1D), two-dimensional (2D) or three-dimensional (3D) periodic arrangement of a dielectric medium. The bandgap response and wave propagation characteristics of the photonic crystal lattice strongly depend on the rods' arrangement, geometry, and material [1], [2]. Furthermore, by introducing defects into photonic crystals, light can be controlled and manipulated, and integrated optical devices can be formed. In photonic crystal structures, cavities can be designed by creating line or point defects. Light is temporarily and spatially confined at the resonant frequency within these cavity structures, known as optical resonators. The optical resonator is a fundamental functional block required for filtering, modulation, buffering, and switching in integrated optical circuit systems [3]. The key components of photonic crystal circuits, such as channel-drop filters and coupled-cavity waveguides, take advantage of defect mode coupling. The effect on the defect mode shift is much more sensitive to a small change in the refractive index than the band edge shift. Applications of photonic crystals can be divided into two types based on the reflective or transmissive nature of the photonic crystal. Light can be easily controlled in photonic crystals as a function of wavelength, enabling the creation of low-loss, wide or narrow bandwidths, and sharp bends equivalents compared to their counterparts [4]. Furthermore, by introducing defects into photonic crystals, light can be controlled and manipulated, and integrated optical devices can be formed [2]. By tuning the configuration of the defect or cavity structure, various functions for advanced signal processing can be realized in all-optical photonic circuits [3]-[5]. Light is temporarily and spatially confined at the resonant frequency within these cavity structures, known as optical resonators. The optical resonator is a fundamental functional block required for filtering, modulation, buffering, and switching in integrated optical circuit systems [3]. The quality factor or Q-factor is an important parameter that determines the performance of a resonant cavity. The photonic microcavity is characterized by the cavity resonant wavelength and the quality factor (Q-factor). The Q-factor is defined as the ratio of the cavity mode wavelength to the cavity mode spectral linewidth [1], [6]. The Q-factor and mode volume are measures of the temporary perturbation time and spatial occupation in the cavity, respectively. In wavelength division multiplexing applications, the Q-factor

and transmission characteristics are important for narrowband filtering [1]. In addition, the strong confinement of light also enhances nonlinear interactions [7]. A designer can change the bandwidth or shape of the frequency response by adjusting the coupling coefficients between the resonances present in the system. As the designer controls the strength of the perturbation, the separation between the two resonant mode frequencies varies accordingly. The key components of photonic crystal circuits, such as channel-drop filters and coupled-cavity waveguides, take advantage of defect mode coupling. The ability to control mode splitting by adjusting the perturbation strength is an important feature of photonic crystal structures. By manipulating the coupling between resonant modes, the designer can engineer the desired spectral response, which is critical for applications such as filtering, switching, and multiplexing in integrated photonic circuits. Defect mode coupling is the underlying principle of many fundamental photonic crystal devices, highlighting the importance of understanding and precisely controlling mode splitting in these periodic dielectric structures. Mode degeneracy in photonic crystal structures is a consequence of the inherent symmetry of the lattice. By deliberately introducing a perturbation, either by a physical change in the cavity or by the addition of an extra element, the mode degeneracy can be removed, leading to mode splitting. This ability to control and tune mode splitting is a valuable feature of photonic crystals, as it enables the engineering of desired spectral responses for applications such as filtering, switching, and multiplexing in integrated photonic circuits. The literature [8]-[11] has explored various approaches to achieving mode splitting, highlighting the flexibility and potential of this technique.

High rotational symmetry photonic crystals exhibit perfectly symmetric ordering. While it simplifies the design and analysis of these structures, it also limits the flexibility to manipulate the optical properties. By reducing the symmetry of the unit cell, low-symmetry photonic crystals (LSPCs) offer greater opportunities for geometric customization and, consequently, greater control over the light-matter interactions. This flexibility is achieved by introducing additional elements or reconfiguring the existing components within the unit cell [12]. The geometric and structural diversities introduced by symmetry reduction in photonic crystal waveguides and cavities enhance the dispersion properties of these periodic materials [13]-[15]. Additionally, low-rotational symmetric photonic crystal structures efficiently manipulate the equifrequency contours, leading to the emergence of self-collimation transmission [16], [17]. The ability to break high symmetry and explore low symmetry designs is featured in the design of photonic crystals to tailor their optical properties for applications such as sensors [18], [19], superprisms [20], and splitters [21]. In this study, the dependence of the degenerate resonance mode on the low-symmetry parameters was investigated, and unlike other studies [10], [11], [22], [23], the intrinsic low-symmetry property of the low-symmetry photonic crystal structure was used to control the resonance modes. To obtain a low-symmetry photonic crystal structure, two rods with different radii were added next to the central rod in a square lattice photonic crystal formed in air, thus breaking the high symmetry of the unit cell (Figure 1). A shoulder-coupled cavity was then created within a linear defect waveguide (LDWG). The splitting and fusing of the cavity modes was studied by varying the position and radius of the low symmetry rods. Mode analysis of the cavity was performed for different radii and positions of the low-symmetry rods, and transmission and reflection spectra were obtained. The results showed that the splitting or merging of the degenerate cavity modes can be controlled by varying the position and/or radius of the low-symmetry rods without the need for additional perturbation. The PWE and FDTD methods implemented in MPB, MEEP and Lumerical software were used to obtain the dispersion behavior and transmission/reflection spectra of the photonic crystal structure. The final experimental study, which is a well-accepted method due to the scalable nature of photonic crystals, was attempted using a microwave experimental setup. However, the measurement results could not be reliably obtained due to the differences between the simulation environment and the experimental setup.

2. Coupled Mode Theory of the Cavity

In photonic crystal structures, two types of optical resonators can be designed: (1) resonators based on line or point defects. For example, a resonator is created by modifying the dimensions or dielectric constant of the rods, resulting in a defect that behaves like a resonator, and (2) ring resonators, where some rods are removed and/or modified to form a ring-shaped resonator. Optical resonators are typically used in conjunction with waveguides and the interaction between them is governed by Coupled Mode Theory (CMT). Optical resonators are divided into two groups related to standing wave (SW) and traveling wave (TW) resonators. Optical communication devices such as filters, add/drops, and multiplexers are realized with the SW or TW type of resonators placed between two optical waveguides. The light signal can be coupled into or dropped from the waveguides via the resonator structure [3]. Optical resonators are typically used in conjunction with waveguides and the interaction between them is governed by Coupled Mode Theory (CMT). In this section, the coupling equations for a standing wave-type direct or indirect shoulder-coupled structure in the waveguide-cavity-waveguide junction are given, and the transmission/reflection plots obtained using MATLAB are presented.

Directly Coupled Cavity: To characterize a directly coupled cavity of the standing wave type, as shown in Figure 1a, it is necessary to define some parameters, namely the resonant frequency or wavelength ω_0 (λ_0); the amplitudes of the incident, transmitted, reflected and dropped waveguide modes

si, st, sr, sd; the perturbation rates $1/\tau_w$ and $1/\tau_i$ due to the coupling loss and the intrinsic loss of the waveguide; the corresponding quality factors Q_w and Q_c; the total quality factor Q_t; the normalized frequency δ; and the transfer functions t, r, d for the transmission, reflection and drop ports, respectively, as given in Eqs. (1-5) [3].

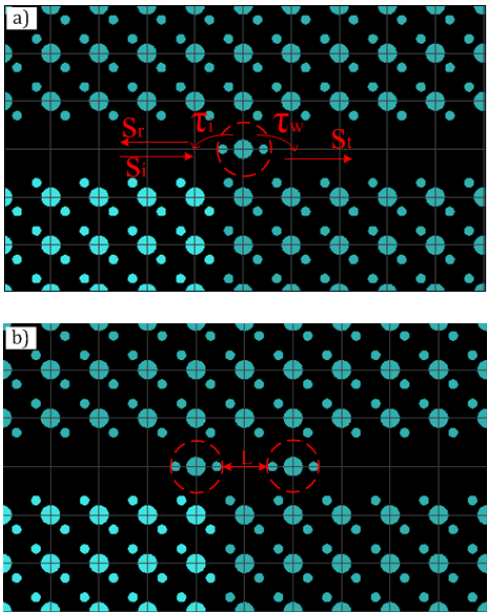

Figure 1. *Low symmetry photonic crystal waveguide with (a) direct or (b) indirect shoulder-coupled standing wave resonator structure.*

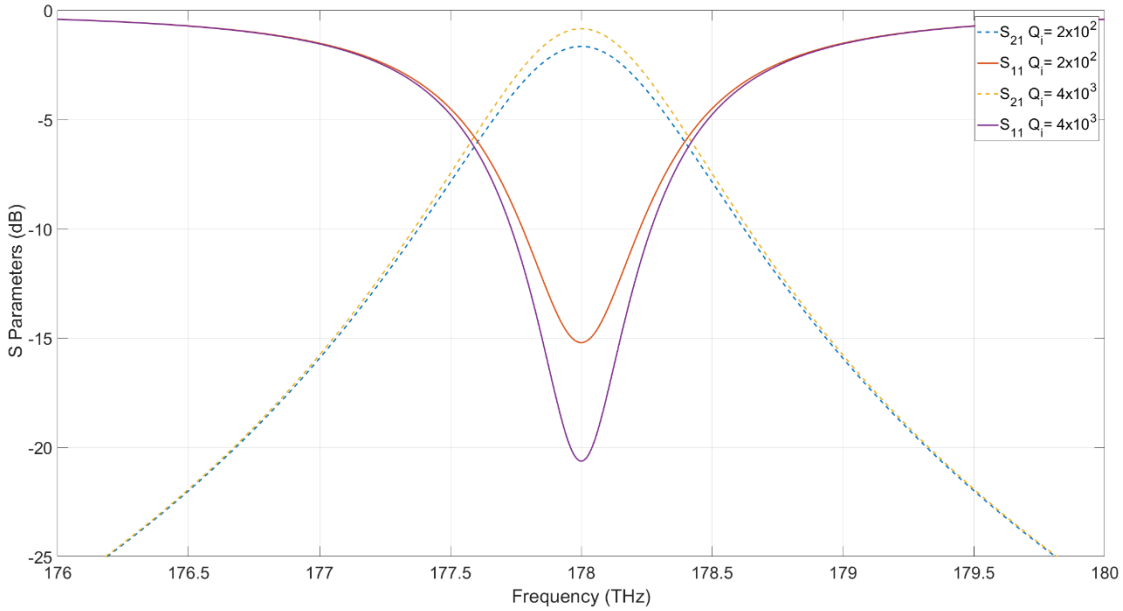

Figure 2. *Transmission and reflection parameters for Qw=2x102 at Qi=2x102 and Qi=4x103 with CMT for standing wave type direct shoulder coupled waveguide-cavity structure*

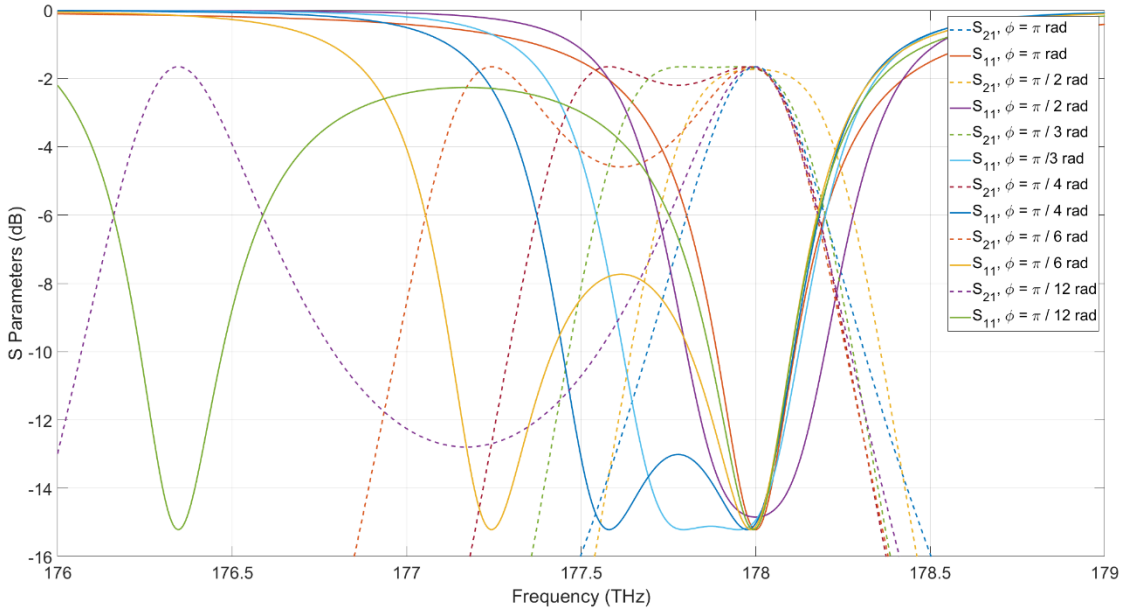

Figure 3. *Transmission/reflection parameters for standing wave type indirectly shoulder coupled waveguide cavity structure with CMT for Qi=4x103, Qw=2x102 at ϕ = pi, pi/2, pi/3, pi/4, pi/6, pi/12 rad phase difference*

$$\delta = \frac{\omega - \omega_0}{\omega_0} \quad (1)$$

$$\frac{1}{Q_t} = \frac{1}{Q_i} + \frac{1}{Q_w} \quad (2)$$

$$t = \frac{st}{si},\ r = \frac{sr}{si},\ d = \frac{sd}{si} \quad (3)$$

$$Q_i = \frac{\omega_0 * \tau_i}{2} \quad (4)$$

$$Q_w = \frac{\omega_0 * \tau_w}{2} \quad (5)$$

For the waveguide-cavity-waveguide configuration, we can use Q_w to represent the total waveguide coupling, so that $Q_w = \omega_0\tau_w$. The term $1/\tau_w$ is the decay rate due to the coupling loss of the waveguide. According to coupled mode theory, the transfer function at the transmit port is given by equation (6) [3]:

$$t = \frac{1/Qw}{j2\delta + 1/Qi + 1/Qw} \quad (6)$$

The transmission T can be calculated as $T = |t|^2$, where θ represents the phase shift and is calculated as θ = arg(t), and τ represents the group delay, calculated as $\tau = d\theta(\omega)/d\omega$. For a waveguide-cavity-waveguide structure supporting a standing wave (SW) cavity, the transmission level approaches unity when the condition Qi ≫ Qw is satisfied, as shown in Figure 2. However, as the Q value increases, the intermodal isolation within the passband decreases, and the mode frequencies approach each other.

The indirectly coupled cavity: This structure, formed by the sequential coupling of two standing wave waveguide-cavity-waveguide systems as shown in Figure 1b, contains two cavity modes due to the presence of two different cavities. This results in a phase shift of ∅ between the cavities. Examining equation (7), the parameter γ represents the transfer function of the reflecting port for a singly coupled standing wave cavity. However, since the system consists of two indirectly coupled cavities, there are two different values of γ.

$$\gamma = \frac{-1}{2Q_w(j\delta + \frac{1}{2Q_i} + \frac{1}{2Q_w})} \quad (7)$$

Since there are two cavities in a cascaded port structure, two different γ values, γ1 and γ2, can be considered. In the transfer function, amplitude transfers for the mirrors are -γ1 and -γ2, while the amplitude reflections are -γ1 - 1 and -γ2 - 1, respectively. The reflection and transmission functions of the whole system can then be obtained from equations (8-9).

$$t = \frac{\gamma_1\gamma_2 e^{j\emptyset}}{1 - (1+\gamma_1)(1+\gamma_2)e^{j2\emptyset}} \quad (8)$$

$$r = \frac{-(1+\gamma_1) + (1+2\gamma 1)(1+\gamma_2)\,e^{j\emptyset}}{1 - (1+\gamma_1)(1+\gamma_2)e^{j2\emptyset}} \quad (9)$$

To simplify the system, if we assume γ1 = γ2, the transfer function of the transmitted port can be rewritten as Equation (10) [3].

$$t = \frac{\frac{1}{8{Q_w}^2 \sin\emptyset}}{(j(\delta + \frac{\cot\frac{\emptyset}{2}}{4Q_w}) + \frac{1}{2Q_i} + \frac{1}{4Q_w})(j(\delta - \frac{\tan\frac{\emptyset}{2}}{4Q_w}) + \frac{1}{2Q_i} + \frac{1}{4Q_w})} \quad (10)$$

The intrinsic quality factor Q_i and the waveguide coupling quality factor are given as $2Q_w$. Since the resonant frequency splitting is highly dependent on ∅, it can only be changed by adjusting ∅. Figure 3 shows that as the phase difference between successive cavities decreases, the mode splits and the bandwidth increases. Conversely, as the phase difference increases, the modes merge again. Analyzing the mode splitting, it is observed that there is critical coupling at a phase difference of π/3 and overcoupling at π/12.

3. Proposed Low-Symmetry Photonic Crystal Cavity Structure and Methodology

This study builds on the low-symmetry structure used in reference [24]. The low-symmetry configuration is created by adding two additional rods at a 45° orientation to a photonic crystal structure consisting of circular cross-section rods arranged in a square lattice on an air substrate. The dielectric constant of both the primary lattice rods and the low-symmetry rods is 12, with radii of r=0.2*a* and rs=0.1*a*, respectively. The low symmetry rods are positioned at a distance of 0.42*a* from the lattice rods. Here "*a*" denotes the lattice constant, with all dimensions and operating frequencies of the photonic crystal normalized accordingly. For example, if *a*=1 μm, then a normalized frequency of 0.4 corresponds to 120 THz.

In the low-symmetry photonic crystal, a waveguide is formed by removing a row of lattice elements arranged in both a linear and a 90-degree bend configuration. In this design, a low-symmetry cavity is placed within the waveguide or at the corner bend region. This cavity structure acts as a coupling element between the waveguides within the low-symmetry photonic crystal structure. The waveguide-cavity coupling utilizes a shoulder coupling configuration operating in the standing wave type. Cases where the dielectric constant of the rods is 12 and 9.61 have been investigated. As a preliminary work, the band diagrams for each low-symmetry photonic crystal lattice were generated. By considering low-symmetry cavity structures, transmission and reflection spectra were obtained by applying various perturbations, such as adding rods, varying rod radii, and changing rod positions within the structure, allowing an analysis of mode splitting. However, this paper only presents results for the linear waveguide configuration with a dielectric constant of 12.

There is no definitive analytical solution for photonic crystal structures containing disorder. The theoretical study of photonic properties in disordered structures is limited to time-consuming numerical simulations. Due to the challenges of analytical approaches, numerical methods are used for the analysis and design of photonic structures. Several methods exist for analyzing the dispersion behavior and transmission spectra of photonic crystals, including the transfer matrix method (TMM) [25], the finite-difference time-domain (FDTD) method [26], the plane wave expansion (PWE) method [27], and the finite element method (FEM) [28], among others. These methods can be divided into frequency domain and time domain calculations. Frequency domain methods are primarily used to calculate band structures, whereas time domain methods are more suitable for evaluating wave propagation and transmission, resonance modes, decay times, etc. Each method has its own strengths and limitations, with PWE and FDTD standing out in terms of performance and meeting the requirements for effective analysis of photonic crystal-based optical devices.

The approach to solving the band structure of a photonic crystal, known as the Plane Wave Expansion (PWE) method, is based on the Fourier expansion of the electromagnetic field and the dielectric function [1], [27]. The PWE method is primarily used for the theoretical analysis of photonic crystal structures, initially using the concept that the eigenmodes in periodic structures can be represented as a superposition of plane waves. The PWE method excels in the calculation of band structure diagrams and modal field patterns. When the original periodicity of the crystal is disturbed, or when a point or line defect appears within the structure, the supercell approach must be applied [1]. Although this method provides an accurate solution for the dispersion properties (propagation modes and photonic band gap) of a photonic crystal, it has certain limitations. Transmission spectra, field distributions and back reflections cannot be derived as only propagation modes are considered. An alternative approach, widely used for the calculation of both transmission spectra and field distributions, is based on the numerical solution of Maxwell's equations via the finite-difference time-domain (FDTD) method. Transmission and reflection spectra are calculated using a numerical FDTD method with Perfectly Matched Layers (PML) or absorbing boundary conditions [26]. Typically, the PWE method is used to calculate the photonic band gap and propagation modes of the photonic crystal structure, while FDTD is used to calculate the transmission spectrum [29]. In this study, the angular position of the low-symmetry rods in the cavity was varied in 15° steps from 0° to 180°, and the rod radius was adjusted between 0.05*a* and 0.1*a* to investigate the transmission characteristics and mode splitting. The transmission characteristics (S-parameters) were obtained and visualized using Lumerical FDTD software. In the final stage, experimental studies were carried out using a microwave setup, exploiting the scalability of

photonic crystals. The physical dimensions of the structure were adapted to the microwave range by exploiting the scalability characteristic of photonic crystals. For example, by choosing a lattice constant of a=15.8 mm, a normalized frequency of 0.4 corresponds to a frequency of 7.5 GHz. Variations in the purity of the dielectric constant of the available rods and inconsistencies in the rod diameters also affected the experimental results. In the experimental setup designed according to the proposed configurations, the S_{21} parameter could be measured with a network analyzer, while accurate S_{11} measurements were difficult. The reasons for this include differences in source placement and type between the experimental and simulation setups. In the simulation, the source is placed directly inside the structure, whereas this is not possible in the microwave measurement setup. In addition, in the simulation the structure is isolated from the external environment and surrounded by a Perfectly Matched Layer (PML), whereas such isolation is not possible in the experimental setup.

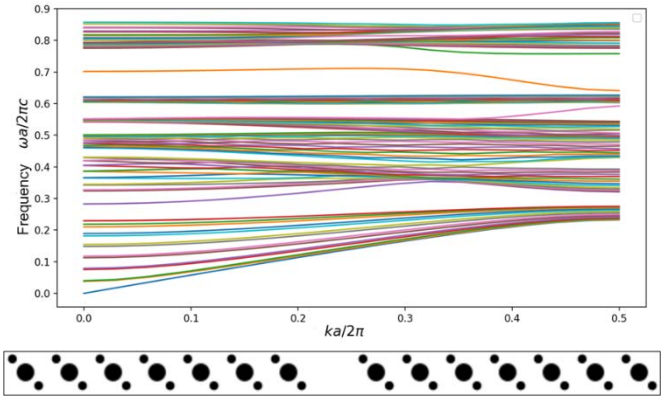

Figure 4. *Supercell structure and TM band diagram of the PC structure with low symmetry linear defect (ε_r=12, Θ: 45°)*

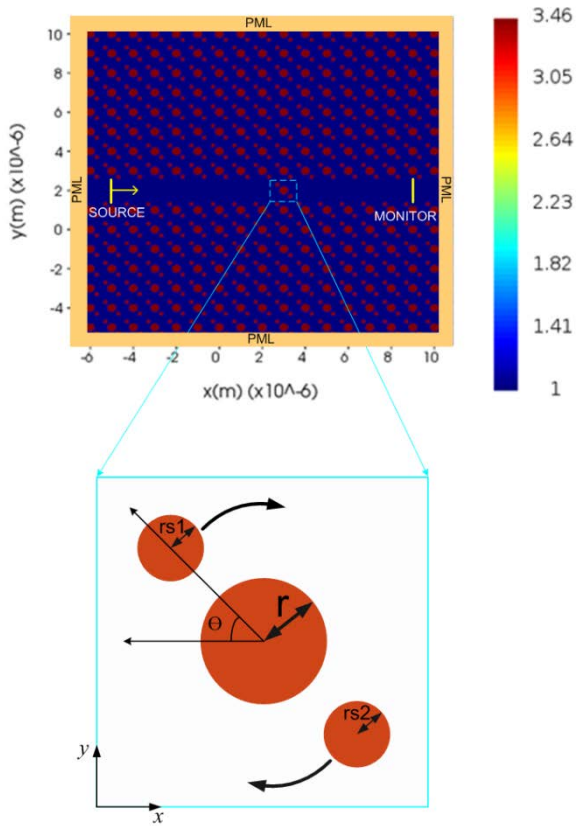

Figure 5. *Simulation schematic and refractive index representation of the cavity structure used with the waveguide in the Low Symmetry PC*

4. Simulation Results and Analysis

In the simulation phase, both direct and indirect coupling configurations were investigated. In the indirect coupling structure, two identical cavities were positioned at a distance of 2a. For the waveguide-cavity coupling configuration, the position and radius of the low-symmetry rods adjacent to the central rod were varied for both cavity types, allowing the transmission coefficient (S_{21}) and reflection coefficient (S_{11}) to be calculated. The angle between the low symmetry rods and the horizontal axis was varied from 0° to 180° in 15° increments. The rod radius was varied from 0 to 0.1a in steps of 0.05a. According to the simulation results, mode splitting and merging can be achieved by simply changing the angular position of the low-symmetry rods, without the need for additional perturbation in the cavity. As the angle of the low-symmetry rod relative to the x-axis increases, the resonant mode frequency splits, resulting in an expanded bandwidth. In addition, the center frequency of the band shifts to lower frequencies.

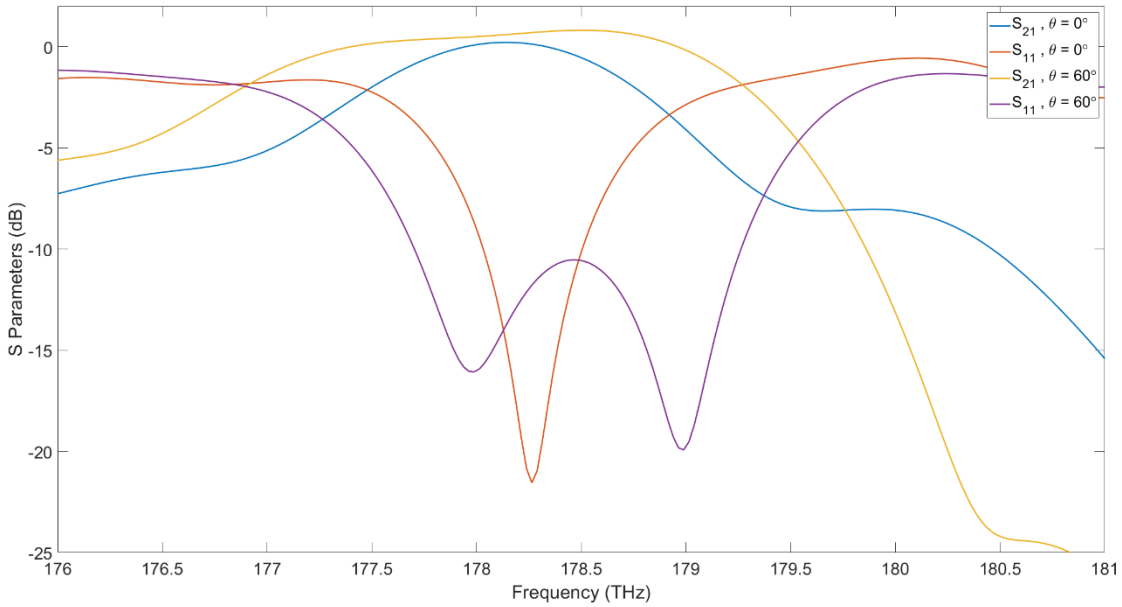

Figure 6. *Transmission/reflection parameters obtained by simulation at different low symmetry rod angle values in direct coupled cavity (rs=0.1a)*

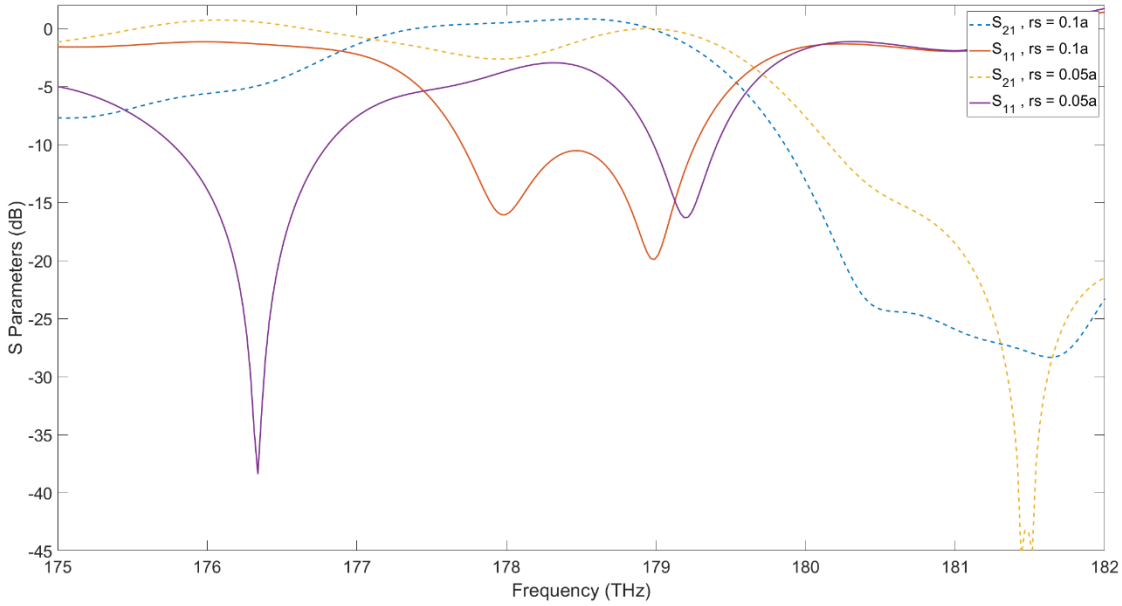

Figure 7. *Transmission/reflection parameters obtained by simulation at different low symmetry rod radius values in direct coupled cavity (Θ=0°)*

4.1 Directly Coupled Cavity

In the simulation results for the directly coupled cavity shown in Figure 6 (corresponding to the structure in Figure 1a), it is observed that the 3dB bandwidth of the band for a single mode is 1.4 THz. As the angle increases, the mode splits and the bandwidth reaches 2.5 THz. At the same angle, mode splitting is observed for both low-symmetry rod radii, with an increase in bandwidth at lower radius values, as shown in Figure 7. Mode analysis of the low-symmetry cavity using the MPB simulation gave the calculated values $Q_i=4\times10^3$ and $Q_w=2\times10^2$. When these values are used with the CMT equations, the results are in good agreement with the simulation, as shown in Figure 8.

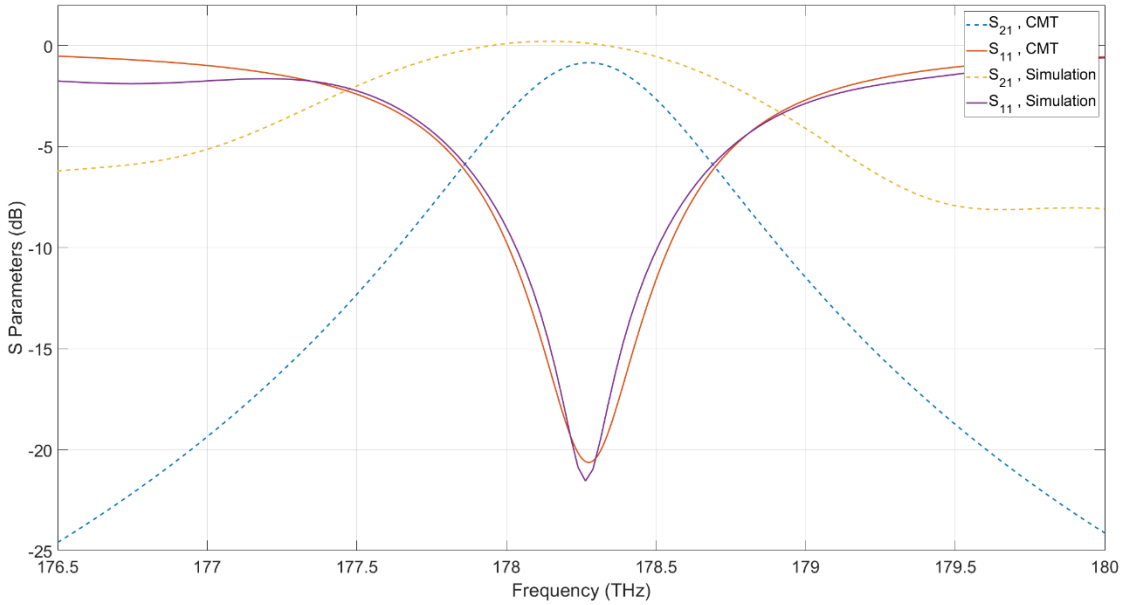

Figure 8. *Comparison of CMT calculation and simulation result (Q_i=4x10^3, Q_w=2x10^2, Θ=0° ve rs=0.1a)*

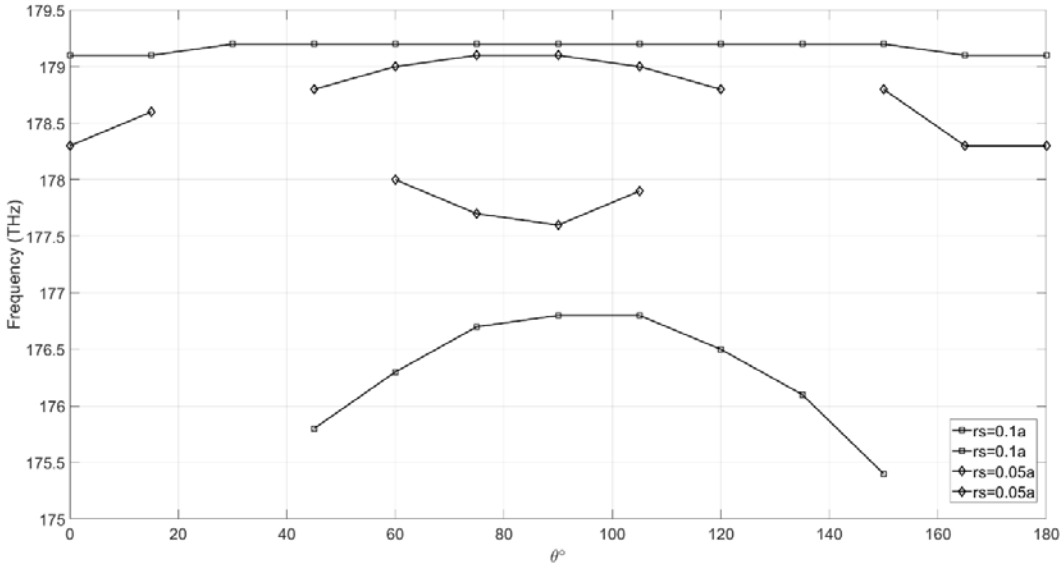

Figure 9. *Variation of mode frequencies at different angle values for rs=0.05a and rs=0.1a in direct coupled structure*

4.2 Indirectly Coupled Cavity

As a further part of the study, the indirectly coupled cavity structure shown in Figure 1b was created using the methodology described in the previous section. Two cavities with equivalent properties were placed 2*a* apart. The angle between the low-symmetry rods and the horizontal axis and the rod radii were varied in both cavities and the transmission/reflection parameters were plotted. In the zero degree configuration, a single mode appeared in the directly coupled structure, while mode splitting occurred in the indirectly coupled structure. However, as the phase difference between the adjacent cavities increased, the modes merged again, as shown in Figure 3. The bandwidth, on the other hand, increased as the phase difference decreased. When the phase difference between the two cavities was $\pi/36$, the comparison

between the CMT calculation and the simulation showed good agreement, as shown in Figure 11. When comparing the CMT and simulation results, shift in mode frequencies is observed in Figure 11 compared to Figure 8. In the indirectly coupled cavity model shown in Figure 1b, the distance between the cavities, enclosed by the red dotted line, is denoted as *L*. However, upon examining each cavity, which consists of primary lattice rods and low-symmetry rods, it becomes evident that each cavity contains a separate defect within itself. This change in distance, and consequently the phase difference, can be considered the cause of the observed shift in the transmission spectrum.

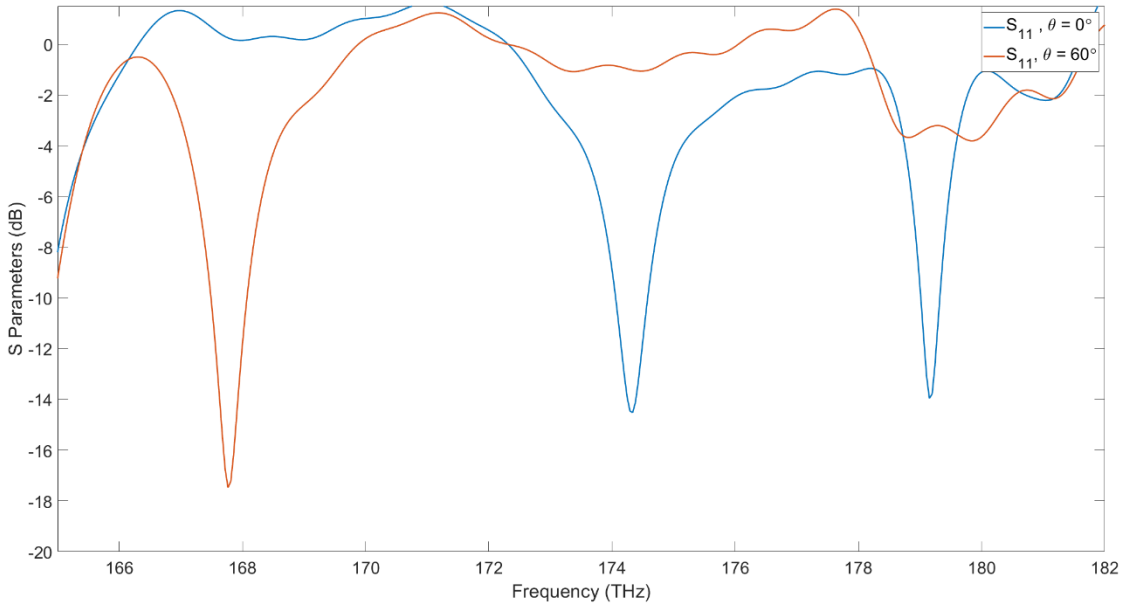

Figure 10. *Reflection parameter obtained by simulation at different low symmetry rod angle values in the indirectly coupled cavity (rs=0.1a)*

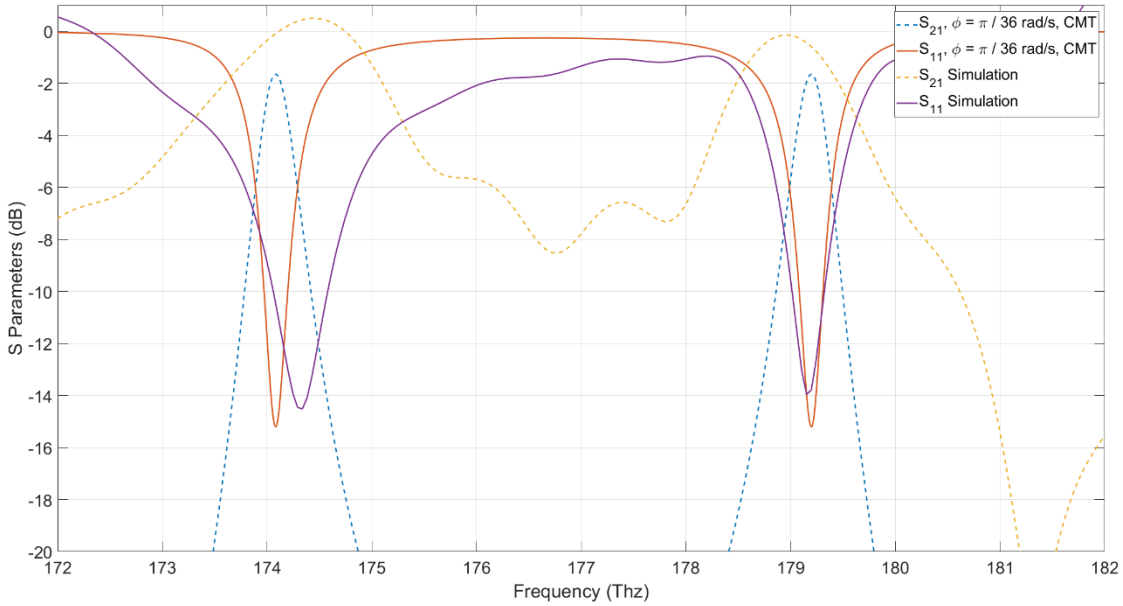

Figure 11. *Comparison of CMT calculation and simulation result in the indirectly coupled cavity (Q_i=4x10^3, Q_w=2x10^2, Θ=0° ve rs=0.1a)*

4.3. Microwave Measurement Setup Proposal

The final stage of the study involved setting up a microwave measurement system for the designed cavity structure to measure the transmission and reflection coefficients. Due to the scalable characteristic of photonic crystals, conducting experiments in the microwave region is an acceptable method in literature. Sub-micron-scale device fabrication and testing require highly costly nanomanufacturing conditions. However, it is also clear that the structures developed for the microwave region cannot be directly applied as photonic devices. Nevertheless, waveguides, splitters, and resonant cavities developed using this technique provide proof of concept essential for advancing our understanding of the interaction between electromagnetic waves and disordered media. In the measurement setup shown in Figure 12, the low-symmetry, direct-coupled, zero-degree configuration cavity structure is shown within a photonic crystal structure consisting of alumina rods arranged in a square lattice. Alumina can be chosen as a dielectric material for the rods, or the rods can be fabricated using 3D printing techniques with materials such as PLA, ABS etc.. In this case, the dielectric constant of the simulated rods should match the dielectric constant of the experimental rods. Since the dielectric constant of the material varies according to the frequency studied, this situation should also be taken into consideration. Additionally, irregularities in the manufacturing process, such as variations in rod diameter or material impurities, can yield erroneous results. To mitigate potential negative effects during measurement, materials with low dielectric constant, such as Plexiglas, can be used as the base plate on which the rods are placed, and the medium can be surrounded by absorber layers. A horn antenna connected to a vector network analyzer was used to apply a source in the range of 8.2 GHz to 12.4 GHz at the input, while the output was measured using an equivalent horn antenna. The scalability property of photonic crystals allows for the frequency range to be adjusted by changing the lattice constant. For example, with a lattice constant of 1.58 cm and 1 μm, the corresponding actual frequencies for a normalized frequency of 0.59 are 11.2 GHz and 177 THz, respectively. In this setup, the lattice constant (a) was selected as 15.8 mm. Accordingly, the actual dimensions of the rods used in the experiment were determined. For instance, a rod with a radius of 0.2a was implemented as a rod with a radius of 3.16 mm. Since two-dimensional (2D) structures effectively represent many scenarios in photonic crystal-based designs, simulations are typically conducted in 2D, with the third dimension considered infinitely long. Adding the third dimension to simulations significantly increases computational time, approximately proportional to the cube of the dimensions. In the experimental setup, the third dimension of the rods is also present. However, rods of about 15 cm or 20 cm in length, which is about eight to ten times the working wavelength, can be acceptable as the infinite length considered in the simulations in this study.

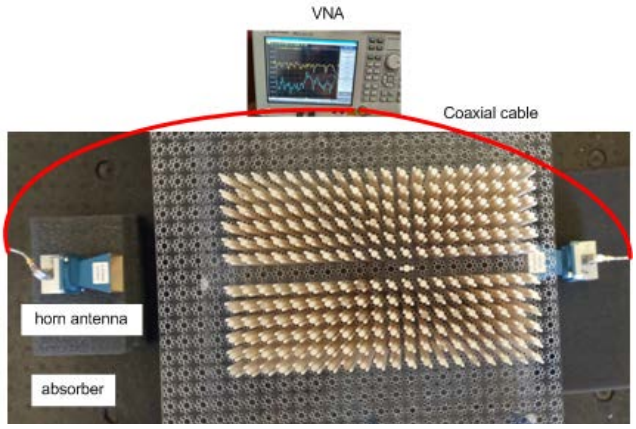

Figure 12. *Experimental setup measured in the microwave region*

The transmission bands observed in the experimental results were consistent with the frequency ranges predicted in the simulations. In this respect, the simulation and experimental results agree. However, deviations in the material parameters and differences between the experimental setup and the simulation environment affected the S-parameter values, leading to inaccuracies. For example, the diameters of the dielectric rods were not uniformly distributed, and their dielectric constants varied due to material impurities. Furthermore, in simulations, the source was placed directly within the structure, but this configuration could not be replicated in the microwave measurement setup. In the simulation environment, the structure was isolated from external influences using a perfectly matched layer (PML), which could not be achieved experimentally. Consequently, the experimental results were excluded from the study.

5. Conclusion

In contrast to traditional high-symmetry structures, low-symmetry photonic crystal structures have opened up a new perspective on light manipulation, offering a wide range of geometric possibilities. This study differs from previous research in that it investigates the effect of angular and dimensional variations in a low-symmetry structure on the cavity resonance mode. The results show that manipulation of the low-symmetry property can lead to the splitting of the resonant mode. The results of this study provide a novel perspective on light transmission and manipulation in low-symmetry photonic crystal structures.

6. Acknowledgements

This study is supported by TUBITAK (The Scientific and Technological Research Council of Turkey) with the project no 118E954. I would like to thank the anonymous referees for their comments.

REFERENCES

[1] Joannopoulos JD, Johnson SG, Winn JN, Meade RD. *Photonic Crystals: Molding the Flow of Light, Second Edition*. New Jersey USA, Princeton University Press, 2008.

[2] Mingaleev S, Kivshar Y. "Nonlinear photonic crystals toward all-optical technologies". *Optics & Photonics News*, 13 (7), 48, 2002.

[3] Li Q, Wang T, Su Y, Yan M, Qiu M. "Coupled mode theory analysis of mode-splitting in coupled cavity system". *Optics Express*, 18 (8), 8367–82, 2010.

[4] Mekis A, Chen JC, Kurland I, Fan S, Villeneuve PR, Joannopoulos JD. "High Transmission through sharp bends in photonic crystal waveguides". *Physical Review Letters*, 77 (18), 3787–3790, 1996.

[5] Fan S, Villeneuve P, Joannopoulos J, Haus H. "Channel drop filters in photonic crystals". *Optics Express*, 3 (1), 4, 1998.

[6] Noble E, Nair RV, Jagatap BN. "Interaction between dual cavity modes in a planar photonic microcavity". *Journal of Modern Optics*, 63 (19), 1981-1991, 2016.

[7] Prorok S. "Nanophotonics and integrated optics photonic crystal cavities". CST Computer Simulation Technology, Darmstadt Germany, whitepaper, 18.04.2013.

[8] Zhang Z, Dainese M, Wosinski L, Qiu M. "Resonance-splitting and enhanced notch depth in SOI ring resonators with mutual mode coupling". *Optics Express*, 16 (7), 4621, 2008.

[9] Mahmoodian S, McPhedran R, Sterke C, Dossou K, Poulton C, Botten L. "Single and coupled degenerate defect modes in two-dimensional photonic crystal band gaps". *Physical Review A*, 79 (1), 013814, 2009.

[10] Daraei A, Khozeymeh F. "Investigation on mode splitting and degeneracy in the L3 photonic crystal nanocavity via unsymmetrical displacement of air-holes". *The International Journal of Engineering and Science*, 2 (2), 146–150, 2013.

[11] Karakilinc OO, Dinleyici MS. "Design of dual-mode dual-band photonic crystal bandpass filters for terahertz communication applications". *Microwave and Optical Technology Letters*, 57 (8), 1806-1810, 2015.

[12] Yuksel ZM, Oguz H, Karakilinc OO, Turduev M, Berberoglu H, Adak M, Kart SO. "Enhanced self-collimation effect by low rotational symmetry in hexagonal lattice photonic crystals". *Physica Scripta*, 99, 065017, 2024.

[13] Turduev M, Giden I. H. , and Kurt H. "Modified annular photonic crystals with enhanced dispersion relations: polarization insensitive self-collimation and nanophotonic wire waveguide designs". *Journal of the Optical Society of America B*, 29(7):1589–1598, 2012.

[14] Gumus M. A., Tutgun M, Yılmaz D, and Kurt H. "A reduced symmetric 2D photonic crystal cavity with wavelength tunability". *Journal of Physics D: Applied Physics*, 52(32):325103, 2019.

[15] Giden I. H., Turduev M., and Kurt H. "Reduced symmetry and analogy to chirality in periodic dielectric media". *Journal of the European Optical Society - Rapid publications*, 9(0), 2014. ISSN 1990-2573.

[16] Giden I. H., Turduev M., and Kurt H. "Broadband super-collimation with low-symmetric photonic crystal". *Photonics and Nanostructures - Fundamentals and Applications*, 11(2):132–138, 2013.

[17] Gumus M., Akcaalan O., and Kurt H. "Crossed chiral band approximation for wide- band self-collimation of light". *Journal of Physics D: Applied Physics*, 53(23):23LT03, 2020.

[18] Erim N., Erim M. N., and Kurt H. "An optical sensor design using surface modes of low-symmetric photonic crystals". *IEEE Sensors Journal*, 19(14):5566–5571, 2019.

[19] Giden I. H. "Photonic crystal based interferometric design for label-free all-optical sensing applications". *Optics Express*, 30(12):21679–21686, 2022.

[20] Gumus M., Giden I. H., and Kurt H. "Enhanced super-prism effect with self-collimation by dispersion management in C1 symmetric photonic crystals". In Ali Adibi, Shawn-Yu Lin, and Axel Scherer, editors, *Photonic and Phononic Properties of Engineered Nanostructures VIII*, 10541, 105411L, SPIE, 2018.

[21] Yasa U. G., Giden I. H., Turduev M., and Kurt H. "Polarization splitting phenomenon of photonic crystals constructed by two-fold rotationally symmetric unit-cells". *Journal of Optics*, 19(9):095005, 2017.

[22] Chun-ping C, Anada T, Greedy S, Benson TM, Sewell P. "A novel photonic crystal band-pass filter using degenerate modes of a point-defect microcavity for terahertz communication". *Microwave and Optical Technology Letters*, 56 (4), 792–797, 2014.

[23] Xia P, Fu Y, Kong M, Liu Z, Zhou J, Zhou J. "Theoretical analysis of the mode splitting properties in periodically patterned microring resonators". *Journal of Lightwave Technology*, 35 (9), 1700-1704, 2017.

[24] Gumus M, Giden HI, Kurt H. "Broadband self-collimation in C2 symmetric photonic crystals". *Optics Letters*. 43, 2555-2558, 2018.

[25] Pendry JB, MacKinnon A. "Calculation of photon dispersion relation", *Physics Review Letters*, 69 (19), 2772-2775, 1992.

[26] Taflove A. *Computational Electrodynamics: The Finite-Difference Time Domain Method*. Boston: Artech House, 2005.

[27] Pendry JB. "Calculating photonic band structure". *Journal of Physics: Condensed Matter*, 8 (9), 1085-1108, 1996.

[28] Pelosi G, Coccioli R, Selleri S. Quick finite elements for electromagnetic waves. Boston USA, Artech House, 1997.

[29] Oskooi AF, Roundy D, Ibanescu M, Bermel P, Joannopoulos JD, Johnson SG. "Meep: A flexible free-software package for electromagnetic simulations by the FDTD method". *Computer Physics Communications*, 181 (3), 687–702, 2010.